Journal of The Electrochemical Society, **158** (9) A1048-A1054 (2011)
0013-4651/2011/158(9)/A1048/7/$28.00 © The Electrochemical Society

Parameter Estimation and Capacity Fade Analysis of Lithium-Ion Batteries Using Reformulated Models

Venkatasailanathan Ramadesigan,[a,*] Kejia Chen,[b] Nancy A. Burns,[c] Vijayasekaran Boovaragavan,[d,] Richard D. Braatz,[b,e] and Venkat R. Subramanian[a,**,z]**

[a]*Department of Energy, Environmental and Chemical Engineering, Washington University, St. Louis, Missouri 63130, USA*
[b]*Department of Chemical and Biomolecular Engineering, University of Illinois, Urbana, Illinois 61801, USA*
[c]*Department of Chemical and Biomolecular Engineering, North Carolina State University, Raleigh, North Carolina 27695, USA*
[d]*Duracell Technology Center, Procter & Gamble, Bethel, CT 06801, USA*
[e]*Department of Chemical Engineering, Massachusetts Institute of Technology, Cambridge, Massachusetts 02139, USA*

Many researchers have worked to develop methods to analyze and characterize capacity fade in lithium-ion batteries. As a complement to approaches to mathematically model capacity fade that require detailed understanding of each mechanism, capacity fade was accurately and efficiently predicted for future cycles using a discrete approach by extrapolating the change in effective transport and kinetic parameters with cycle number (N) for a battery tested under controlled experimental conditions. The effective parameters and their uncertainties are estimated using a mathematical reformulation of a porous electrode model, whose computational efficiency enables the integration of the proposed approach into an inexpensive microprocessor for estimating the remaining lifetime of a battery based on past charge-discharge curves. The approach may also provide some guidance for designers as to which battery components to focus on for redesign to reduce capacity fade.
 [DOI: 10.1149/1.3609926]

Manuscript submitted September 22, 2010; revised manuscript received May 9, 2011. Published July 20, 2011. *This was Paper 251 presented at the San Francisco, California Meeting of the Society May 24–29, 2009.*

Electrochemical power sources appear in applications in automobiles, power storage, military, mobile applications, and space. Lithium-ion chemistry has been identified as a preferred candidate for high-power/high-energy secondary batteries. Significant progress has been made in developing lithium-ion battery models that incorporate transport phenomena, electrochemical kinetics, and thermodynamics.[1–8] While these models have been used to produce reliable predictions for a small number of cycles, their ability to predict the reduction in capacity during cycling is limited. Different mechanisms causing capacity fade include (i) capacity fade during formation cycles, (ii) overcharging, which results in a decrease in capacity in both positive and negative electrodes and the electrolyte, (iii) decomposition of the electrolyte during the reduction process, (iv) self-discharge depending on the purity of materials used in manufacturing, and (v) formation of a passive film on the electrode that grows in thickness as the cycle number increases.[5,7] Figure 1 shows the region in which each phenomenon occurs within a battery. Table I lists some of the mechanisms causing capacity fade and the possible parameters that could be affected in a pseudo-2D porous-electrode-based model of a lithium-ion battery.

In some recent work, Safari et al.[9,10] assessed the possibility of using a mechanical-fatigue life-prognostic method for the life prediction of lithium-ion batteries. This method was successfully demonstrated for predicting the capacity loss but is limited by the choice between the time frame of the aging experiments and the life-prediction accuracy. In addition, the method is an empirical tool, which has its own limitations. Yoshida et al.[11] fabricated a lithium-ion cell with 5-Ah capacity, fitted experimental data on the thickness of the SEI layer growth, and demonstrated that their empirical fit predicted the life under certain conditions. Other recent efforts have developed more efficient simulation techniques for phenomenological models of capacity fade.[4,12] A complete phenomenological model for capacity fade has not been forthcoming due to (i) incomplete understanding of all of the capacity fade mechanisms, (ii) lack of knowledge for the values of the model parameters in these mechanisms, (iii) difficulties in obtaining these parameter values due to cumulative non-separable effects of individual mechanisms occurring simultaneously, and (iv) numerical inability and lack of efficient numerical solvers to be able to solve the complex models efficiently with proper state detections. Oftentimes in the quest for adding detailed mechanisms, researchers have neglected important electrochemical/transport phenomena typically in porous electrode-based battery models. For example, researchers have employed simpler single-particle models or empirical fits that neglect important electrochemical/transport phenomena to accommodate the increased complexity of capacity fade mechanisms. Today very few phenomenological models include mechanisms for capacity fade in Li-ion batteries[8,12] and no models include all of the postulated mechanisms.

This paper proposes an alternative approach to the estimation of the life of a battery, which uses voltage-discharge curves measured during initial cycles to predict voltage-discharge curves during later cycles. A model reformulation[4] is employed to efficiently extract the effective kinetic and transport parameters from experimental data, with uncertainties in parameters and model predictions quantified using established analysis techniques. The next sections describe the lithium-ion battery model used in this study, the numerical algorithms used to implement the discrete approach to capacity fade prediction, the results and discussion, and the conclusions.

Lithium-Ion Battery Model and Simulation

Phenomenological battery models typically solve electrolyte concentration, electrolyte potential, solid-state potential, and solid-state concentration in the porous electrodes and electrolyte concentration and electrolyte potential in the separator regions.[1,2] These models are represented by coupled nonlinear partial differential equations in one, two, or three dimensions, are typically solved numerically, and require a few seconds to minutes to simulate. Simulation of lithium-ion battery models requires simultaneous evaluation of concentration and potential fields, both in the solid and electrolyte phases. The porous nature of the battery electrodes leads to highly nonlinear and heterogeneous electrochemical reaction kinetics. A pseudo-two-dimensional (P2D) model developed by Doyle et al.[6] is considered in this work. The governing equations in the full physics-based P2D model for the five variables Φ_1, Φ_2, c, c_s^{ave}, and j_p that vary with x are given in Table II. Usually lithium-ion battery models are numerically simulated by finite-difference discretization of all the variables in the spatial coordinates. The discretization of the cathode, separator, and anode into 50 equally spaced node points would result in 600 Differential Algebraic Equations (DAEs) to be solved in the finite difference model, which is

* Electrochemical Society Student Member.
** Electrochemical Society Active Member.
z E-mail: vsubramanian@seas.wustl.edu

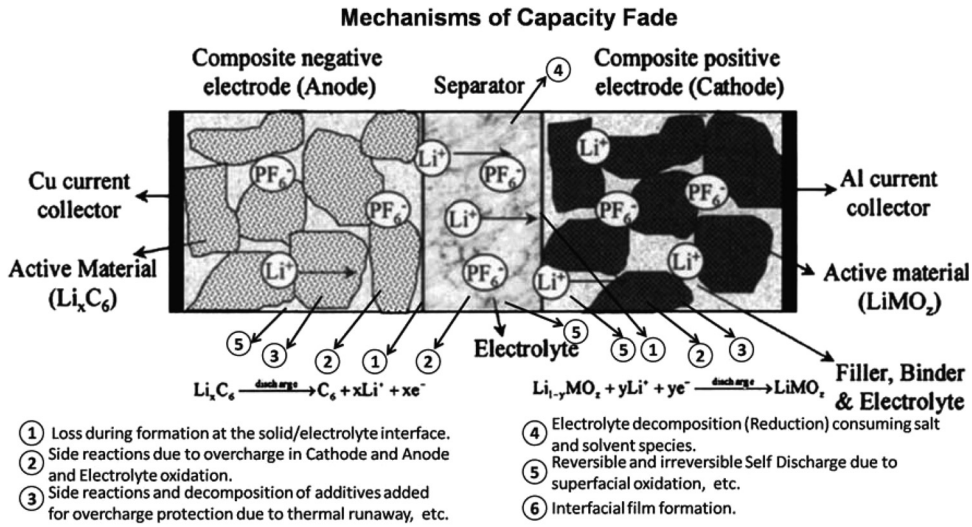

Figure 1. A schematic of some capacity fade mechanisms postulated in a Li-ion battery.

impractical for real-time simulation. Parameter estimation and optimization of lithium-ion battery, where the life and health of the battery is vital to the operation of the device, requires quick-solving models that can give an accurate account of the battery variables. A model reformulation[4] of the P2D model[6] was developed by exploiting the mathematical structure of the DAEs while conserving mass, charge, and current in each electrode and having much lower memory requirements and computational costs compared to standard finite-difference methods. The details on the reformulation of the P2D model are provided elsewhere.[4]

The accuracy and simplicity of the reformulated model enables an easy computation of parameter sensitivities and even numerical jacobians are likely to be more accurate and stable compared to the direct finite-difference method applied to the original P2D model. These features of the model reformulation were utilized during the parameter estimation described in Parameter estimation section to extract effective kinetic and transport parameters from experimentally measured voltage-discharge curves. The reformulated model also enabled the application of the Markov Chain Monte Carlo (MCMC) method, as described in Uncertainty quantification section, to quantify the magnitude of uncertainties in the model parameters.

Numerical Algorithms

This section describes the discrete approach to capacity fade prediction and the parameter estimation and uncertainty quantification methods used in the implementation of the discrete approach.

Discrete approach to capacity fade prediction.—This paper reports a discrete parameterized approach to predict capacity fade in Li-ion batteries. The variations in effective transport and kinetic parameters are tracked with discharge curves at different cycles as described in Parameter estimation section. The estimated parameters were the effective diffusion coefficient of lithium ion in the solution phase (D_1), effective diffusion coefficient of lithium in the solid phase for the negative and positive electrodes (D_{sn} and D_{sp}), and electrochemical reaction rate constants for the negative and positive electrodes (k_n and k_p). Note that the effective diffusion coefficient through porous media is a function of a species' molecular diffusion coefficient and the porosity, tortuosity, and constrictivity of the media,[13] which change as a battery ages, so that the effective diffusion coefficient changes with cycle #. The electrochemical rate constants are also *effective*, in that they are a function of the true electrochemical rate constant and the surface area available for electrochemical reaction, which will decrease as alloys are formed on the electrode surface that block or hinder electrochemical reaction. In an application to a U.S. Government battery, Results and Discussion section demonstrates that power-law extrapolation of the change in the effective transport and kinetic parameters predicted the future voltage-discharge curves and the life of the battery.

Uncertainty quantification methods are applied to avoid overfitting of the model parameters to the experimental data. Uncertainties in the effective model parameters are quantified as described in Uncertainty quantification section, and used to reduce the set of estimated model parameters to include only those parameters that can be estimated with sufficient accuracy from the experimental data. Uncertainties in the model predictions are also quantified, with the 95% predictive intervals for future cycles compared with the experimental data in Results and Discussion section.

Parameter estimation.—The model parameter estimates were obtained by the solution of a nonlinear optimization that minimizes the sum-of-squared differences between the model outputs and their experimentally measured values for each cycle i[14–16]

$$\min_{\theta_i} \sum_{j=1}^{n_i} \left[y_i(t_j) - y_{model,i}(t_j; \theta_i) \right]^2 \quad [1]$$

where $y_i(t_j)$ is the measured voltage at time t_j for cycle i, $y_{model,i}(t_j; \theta_i)$ is the voltage computed from the reformulated model at time t_j for cycle i for the vector of model parameters θ_i (the five parameters being the effective solid-phase diffusion coefficient and

Table I. List of capacity fade mechanisms and possibly affected parameters in a pseudo-2D model.

Mechanism of capacity fade	Possible affected parameters
Capacity fade during formation cycles	x_{p0}, x_{n0}, ε_p, ε_n, D_{sp}, D_{sn}, k_p, k_n
Overcharging that results in decrease in capacity in both positive and negative electrodes	D_{sp}, D_{sn}, k_p, k_n
Decomposition of the electrolyte during the reduction process	D_1, k_p, k_n
Self-discharge depending on the purity ofmaterials used in manufacturing	D_{sp}, D_{sn}, k_p, k_n
Formation of a passive film on the electrode that grows in thickness as the cycle number increases	k_s, R_{film}
Loss of active material during cycling	x_{p0}, x_{n0}, ε_p, $\varepsilon_{n,}$ $\varepsilon_{f,p}$, $\varepsilon_{f,n}$

reaction rate constant in each electrode and solution-phase diffusion coefficient of the electrolyte), and n_i is the number of time points in cycle i. Solving the optimization [1] is known in the literature as *least-squares estimation*.[14–16] Many numerical algorithms are available for solving the nonlinear optimization [1], such as the steepest descent, Gauss-Newton, and Marquardt methods.[14] In this work, the Gauss-Newton method[14] was applied to estimate parameters using the reformulated model. For the least-squares estimation, this Jacobian-based method is an iterative process that reduces the sum-of-squared differences between the model outputs and the experimental data points until the error is no longer significantly reduced.

Uncertainty quantification.— Uncertainties in the model parameter estimates were quantified by three methods: (i) estimation of hyper-ellipsoidal 95% confidence regions by applying Chi-squared statistics to a Taylor series expansion between the model parameters and the model outputs,[15,16] (ii) estimation of 95% confidence regions by applying F-statistics to the parameter estimation objective function [1],[15,16] and (iii) estimation of probability distributions using the Markov Chain Monte Carlo (MCMC) method.[17,18] The first two methods, which are the most commonly applied in the literature, gave highly inaccurate confidence regions for this application, whereas the MCMC method is a very accurate method for uncertainty quantification for any application. The MCMC method employs a Monte Carlo sampling method to numerically construct the probability distribution for each model parameter and cycle i from the posterior distribution for the parameter estimates obtained using Bayes' rule[17,18]

$$\Pr(\theta_i|Y_i) = \frac{\Pr(Y_i|\theta_i)\Pr(\theta_i)}{\Pr(Y_i)} \quad [2]$$

where Y_i was the vector obtained by stacking the voltage measurements $y_i(t_j)$, $\Pr(\theta_i)$ is the prior distribution of θ_i which was specified as a uniform distribution with a width of 20% centered at the parameters estimated using the least-squares method [1], $\Pr(Y_i|\theta_i)$ is the likelihood of obtaining the data Y_i given parameters θ_i, and $\Pr(Y_i)$ is a normalization constant so that the posterior distribution $\Pr(\theta_i|Y_i)$ integrates to unity. The term $\Pr(Y_i|\theta_i)$, which is known as the *likelihood function*, for this application is

$$\prod_{j=1}^{n_i} \frac{1}{\sqrt{2\pi}\sigma_\varepsilon} \exp\left(\frac{(y_i(t_j) - y_{model,i}(t_j;\theta_i))^2}{2\sigma_\varepsilon^2}\right) \quad [3]$$

where $\sigma_\varepsilon = 0.01$V was the standard deviation of the voltage measurement noise. The probability distribution for each model parameter is equal to integrals of the posterior distribution [2] over the other model parameters. Unlike the conventional Monte Carlo method for computing integrals,[19] the samples in the MCMC method are correlated; generating what is known as a *Markov chain*, whose probability distribution approaches the probability distribution for each parameter. More detailed descriptions are provided in the Refs. 17 and 18.

Other advantages of the MCMC method are its explicit consideration of constraints and arbitrary non-Gaussian distributions for

Table II. Governing equations for a lithium-ion battery (published as Table 1 of Ref. 4).

Region	Eq. #	Governing equations	Boundary conditions
Positive electrode	T1	$\varepsilon_p \frac{\partial c}{\partial t} = D_{eff,p}\frac{\partial^2 c}{\partial x^2} + a_p(1-t_+)j_p$	$-D_{eff,p}\left.\frac{\partial c}{\partial x}\right\|_{x=0} = 0$ & $-D_{eff,p}\left.\frac{\partial c}{\partial x}\right\|_{x=l_p,-} = -D_{eff,s}\left.\frac{\partial c}{\partial x}\right\|_{x=l_p,+}$
		initial condition $c\|_{t=0} = c_0$	
	T2	$-\sigma_{eff,p}\frac{\partial \Phi_1}{\partial x} - \kappa_{eff,p}\frac{\partial \Phi_2}{\partial x} + \frac{2\kappa_{eff,p}RT}{F}(1-t_+)\frac{\partial \ln c}{\partial x} = I$	$-\kappa_{eff,p}\left.\frac{\partial \Phi_2}{\partial x}\right\|_{x=0} = 0$ & $-\kappa_{eff,p}\left.\frac{\partial \Phi_2}{\partial x}\right\|_{x=l_p,-} = -\kappa_{eff,s}\left.\frac{\partial \Phi_2}{\partial x}\right\|_{x=l_p,+}$
	T3	$\sigma_{eff,p}\frac{\partial^2 \Phi_1}{\partial x^2} = a_p F j_p$	$\left.\frac{\partial \Phi_1}{\partial x}\right\|_{x=0} = -\frac{I}{\sigma_{eff,p}}$ & $\Phi_1 = 4.2$
	T4	$\frac{d}{dt}c_s^{ave} + 3\frac{j_p}{R_p} = 0$ & $\frac{D_{s,p}}{R_p}(c_s^{surf} - c_s^{ave}) = -\frac{j_p}{5}$	$c_s^{ave}\|_{t=0} = c_{s,max,p}$
Separator	T5	$\varepsilon_s \frac{\partial c}{\partial t} = D_{eff,s}\frac{\partial^2 c}{\partial x^2}$	$-D_{eff,p}\left.\frac{\partial c}{\partial x}\right\|_{x=l_p,-} = -D_{eff,s}\left.\frac{\partial c}{\partial x}\right\|_{x=l_p,+}$ & $-D_{eff,s}\left.\frac{\partial c}{\partial x}\right\|_{x=l_p+l_s,-} = -D_{eff,n}\left.\frac{\partial c}{\partial x}\right\|_{x=l_p+l_s,+}$
	T6	$I = -\kappa_{eff,s}\frac{\partial \Phi_2}{\partial x} + \frac{2\kappa_{eff,s}RT}{F}(1-t_+)\frac{\partial \ln c}{\partial x}$	$-\kappa_{eff,p}\left.\frac{\partial \Phi_2}{\partial x}\right\|_{x=l_p,-} = -\kappa_{eff,s}\left.\frac{\partial \Phi_2}{\partial x}\right\|_{x=l_p,+}$ & $-\kappa_{eff,s}\left.\frac{\partial \Phi_2}{\partial x}\right\|_{x=l_p+l_s,-} = -\kappa_{eff,n}\left.\frac{\partial \Phi_2}{\partial x}\right\|_{x=l_p+l_s,+}$
Negative electrode	T7	$\varepsilon_n \frac{\partial c}{\partial t} = D_{eff,n}\frac{\partial^2 c}{\partial x^2} + a_n(1-t_+)j_n$	$-D_{eff,s}\left.\frac{\partial c}{\partial x}\right\|_{x=l_p+l_s,-} = -D_{eff,n}\left.\frac{\partial c}{\partial x}\right\|_{x=l_p+l_s,+}$ & $-D_{eff,n}\left.\frac{\partial c}{\partial x}\right\|_{x=l_p+l_s+l_n} = 0$
		initial condition $c\|_{t=0} = c_0$	
	T8	$-\sigma_{eff,n}\frac{\partial \Phi_1}{\partial x} - \kappa_{eff,n}\frac{\partial \Phi_2}{\partial x} + \frac{2\kappa_{eff,n}RT}{F}(1-t_+)\frac{\partial \ln c}{\partial x} = I$	$-\kappa_{eff,s}\left.\frac{\partial \Phi_2}{\partial x}\right\|_{x=l_p+l_s,-} = -\kappa_{eff,n}\left.\frac{\partial \Phi_2}{\partial x}\right\|_{x=l_p+l_s,+}$ & $\left.\frac{\partial \Phi_2}{\partial x}\right\|_{x=l_p+l_s+l_n} = 0$
	T9	$\sigma_{eff,n}\frac{\partial^2 \Phi_1}{\partial x^2} = a_n F j_n$	$-\sigma_{eff,n}\left.\frac{\partial \Phi_1}{\partial x}\right\|_{x=l_p+l_s} = 0$ & $\left.\frac{\partial \Phi_1}{\partial x}\right\|_{x=l_p+l_s+l_n} = -\frac{I}{\sigma_{eff,n}}$
	T10	$\frac{d}{dt}c_s^{ave} + 3\frac{j_n}{R_n} = 0$ & $\frac{D_{s,n}}{R_n}(c_s^{surf} - c_s^{ave}) = -\frac{j_n}{5}$	$c_s^{ave}\|_{t=0} = c_{s,max,n}$

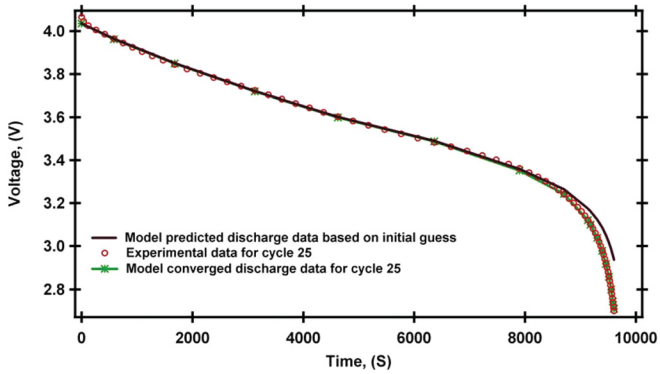

Figure 2. (Color online) Comparison of voltage-discharge curves from the battery models with the experimental data, with five model parameters obtained from least-squares estimation applied to the experimental data for cycle 25. The voltage-discharge curve for cycle 0, which was the same for the finite-difference model and reformulated model, was used as the initial guess.

prior knowledge on the parameters, and that it exactly handles the full nonlinearity in the model equations. For an accurate quantification of the uncertainties, the MCMC method requires many simulation runs, which was facilitated by use of the reformulated model.

The effect of the parameter uncertainties on the accuracy of the predictions of the lithium-ion battery model was also quantified. Although the reformulated model was computationally efficient enough for the standard Monte Carlo method to be applied to quantify the accuracy of the model predictions, the computational cost was further reduced by replacing the reformulated model with a polynomial series expansion[20,21] during the computation of the prediction intervals. The application of this approach to electrochemical and materials systems is described in great detail in the literature.[22–25]

Results and Discussion

The experimental data for the analysis were obtained for U.S. Government BTE cells and chemistry.[26,27] Five effective transport and kinetic parameters were estimated by applying least-squares estimation to the U.S. Government BTE cells experimental voltage-discharge data. The standard finite-difference model and the reformulated model gave the same voltage-discharge curves at cycle 0 (see Fig. 2). Using the model parameters at cycle 0 as an initial guess, Fig. 2 compares the experimental voltage-discharge curve at cycle 25 with the reformulated model output obtained using five model parameters fit by least-squares estimation to that experimental data set. Similar parameter estimations and fits were obtained for later cycle numbers (50 and 100n where $n = 1 \ldots 10$).

The expected monotonic reduction in capacity with cycle # is shown in the voltage-discharge curves obtained by fitting the five model parameters to experimental data (see Fig. 3a). The mechanisms of capacity fade and its overall reduction in battery performance (see Fig. 1) suggest that all five effective model parameters should decrease monotonically with cycle #. The effective negative-electrode solid-phase diffusion coefficient and reaction rate constant (D_{sn} and k_n) decrease monotonically with cycle #, whereas the other

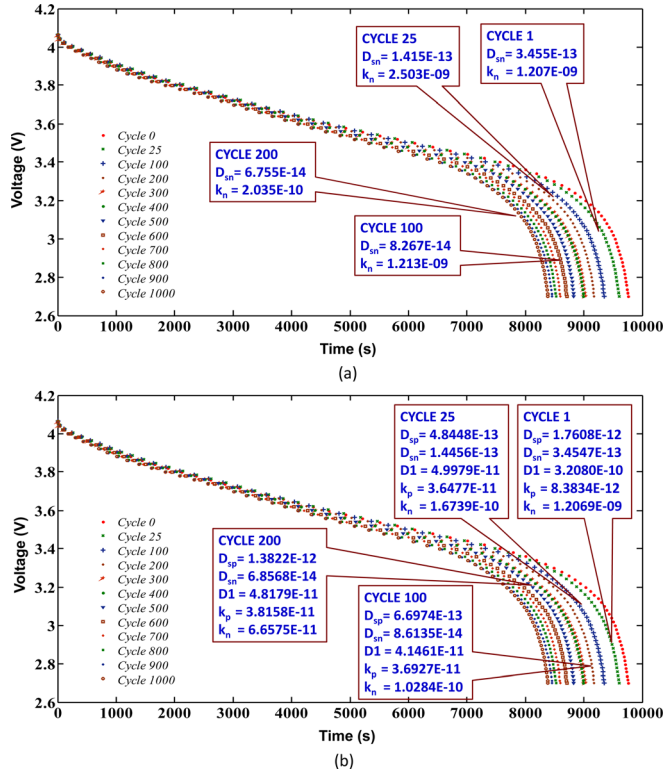

Figure 3. (Color online) Voltage-discharge curves for the U.S. Government BTE cells with model parameters obtained from least-squares estimation applied to the experimental data for (a) five parameters, (b) two parameters. The voltage-discharge curves for the models fall on top of the experimental data so only one set of curves are plotted. The curves shift towards the left monotonically as the cycle # increases.

three parameters did not follow any particular trend (see Fig. 3a). This suggested that the voltage-discharge curves may not contain sufficient information to accurately estimate the effective values of D_1, D_{sp}, and k_p, and that the change in the voltage-discharge curves with cycle # could be captured by estimation of only the effective solid-phase diffusion coefficient D_{sn} and reaction rate constant k_n for the negative electrode. The voltage-discharge curves could be fit using just the two model parameters D_{sn} and k_n, which had to significantly change their values to be able to fit the voltage-discharge curves at higher cycle number (see Fig. 3b).

An initially surprising observation was that, when only two model parameters were fit, the effective reaction rate constant k_n was not monotonically decreasing with cycle # between cycle 0 and cycle 25 (see Fig. 3b). This observation motivated a more detailed analysis by application of sensitivity analysis and the MCMC method. The voltage-discharge curves were very sensitive to the value of the effective solid-phase diffusion coefficient D_{sn} but weakly sensitive to deviations in the model parameters D_1, D_{sp}, k_p, and k_n from their nominal values, resulting in large uncertainties in their values when fit to

Table III. Estimated uncertainty ranges for the four least-sensitive battery model parameters.

Cycle #	D_{sp}	k_n	D_1	k_p
1	$[-60\%, +20\%]$	$[-60\%, +20\%]$	$[-60\%, +20\%]$	$[-10\%, +10\%]$
100	$[-60\%, +20\%]$	$[-60\%, +20\%]$	$[-20\%, +60\%]$	$[-10\%, +10\%]$
200	$[-60\%, +30\%]$	$[-60\%, +20\%]$	$[-20\%, +40\%]$	$[-10\%, +10\%]$
300	$[-30\%, +60\%]$	$[-20\%, +60\%]$	$[-30\%, +60\%]$	$[-10\%, +10\%]$
500	$[-60\%, +60\%]$	$[-20\%, +20\%]$	$[-60\%, +60\%]$	$[-10\%, +10\%]$
600	$[-60\%, +30\%]$	$[-20\%, +20\%]$	$[-60\%, +10\%]$	$[-10\%, +10\%]$
1000	$[-20\%, +60\%]$	$[-10\%, +60\%]$	$[-20\%, +60\%]$	$[-5\%, +5\%]$

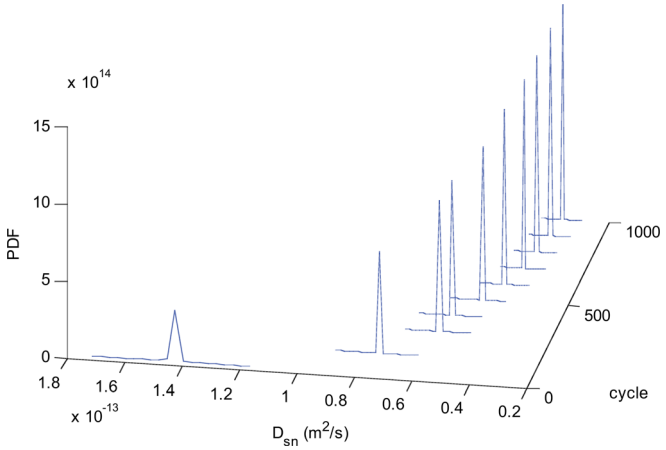

Figure 4. (Color online) Probability density function (pdf) for the effective solid-phase diffusion coefficient D_{sn} at the negative electrode as a function of cycle number determined by the MCMC method.

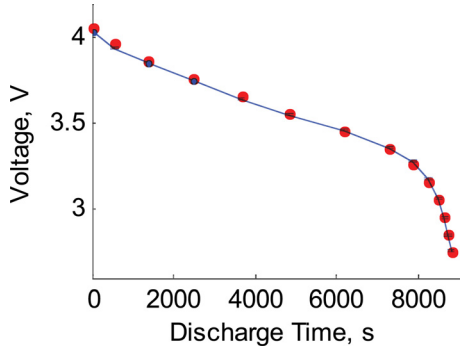

Figure 6. (Color online) Comparison of the experimental voltage-discharge curve with the model prediction with estimated parameters for cycle 500. Each red dot is a data point, the blue line is the model prediction, and the 95% predictive intervals were computed based on the parametric uncertainties quantified by pdfs of the model parameters.

experimental voltage-discharge curves (see Table III). The nominal estimate of the effective solid-phase diffusion coefficient D_{sn} monotonically decreases with increased cycle number (see Fig. 3b), with the nominal estimates being highly accurate according to the probability density function (pdf) computed by the MCMC method (see Fig. 4). The pdfs for D_{sn} at different cycle numbers have minimal overlap, providing very high confidence that the monotonic reduction of the effective solid-phase diffusion coefficient with increase cycle number is statistically significant. That the voltage-discharge curves were much sensitive to a negative-electrode parameter (D_{sn}) suggests that mechanisms for capacity fade in the negative electrode, rather than the electrolyte or positive electrode, were the most important for this battery under these operating conditions. The pdfs of the other model parameters are sufficiently broad (see Table III) that an observed increase in a model parameter from one cycle to the next, as seen in Fig. 3b, may not be statistically significant.

The overall trend in the variation of model parameters is more reliably assessed by plotting nominal estimates over many cycles. A discrete approach was adopted for the prediction of capacity fade by tracking the change in effective transport and kinetic parameters with cycle number (N). Figure 5 shows the variation with cycle number of the effective diffusion coefficient D_{sn} and electrochemical reaction rate constant k_n for the negative electrode. Power laws are commonly used to fit the decay of a property,[28] which motivated the estimation of the model parameters and computation of the voltage-discharge curve at cycle 600 by extrapolation of power-law fits for the variations in each model parameter as a function of cycle number for 25, 50, 100, and 200. The mathematical model produces accurate predictions of the voltage-discharge curve at cycles 500 and 600 (see Figs. 5 and 6).

The model parameters D_{sn} and k_n fit to the experimental data for cycles 50, 100, 200, 300, 400, and 500 were used to predict the remaining battery life based on voltage-discharge curves measured in past cycles. To characterize the degradation in the model parameters, a power law was fit to the estimated parameter values from cycles 25–500 similar to what was done for least-squares estimation. Implicitly assuming that the changes in the parameter values are the result of the same mechanism in later cycles, the parameter values for the subsequent cycles were predicted using the power-law expressions. The voltage-discharge curve predicted by this model was in very

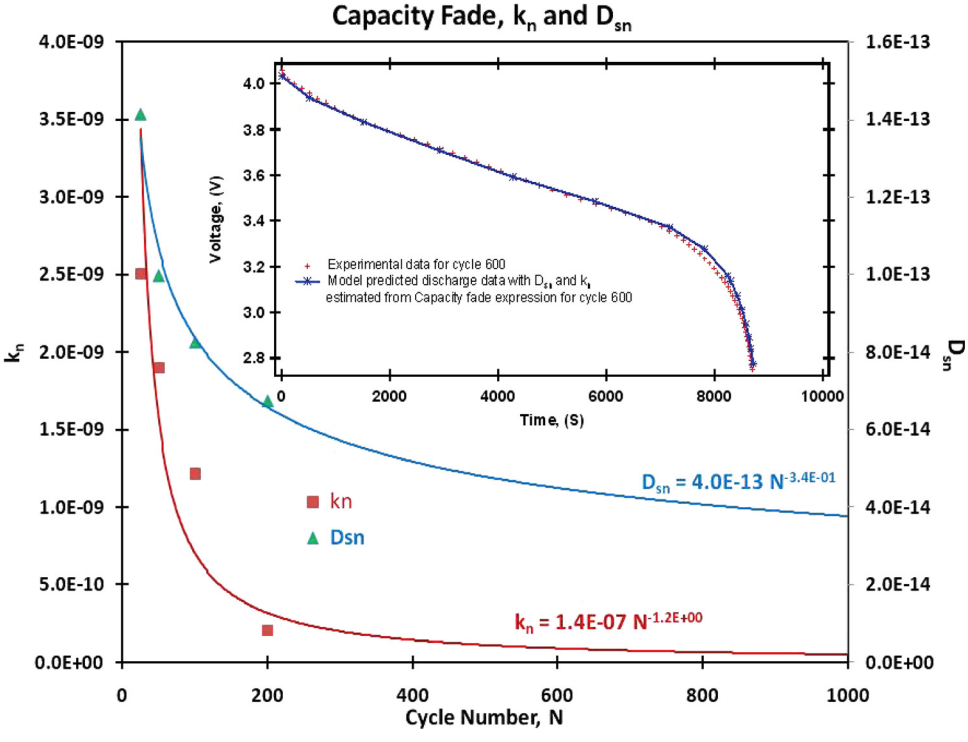

Figure 5. (Color online) Variations in the effective solid-phase diffusion coefficient D_{sn} and electrochemical reaction rate constant k_n at the negative electrode. The inset plot compares the experimental data at cycle 600 with model prediction in which model parameters were extrapolated from power-law fits to model parameters estimated only up to cycle 200.

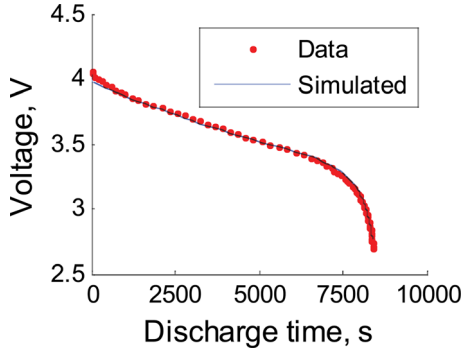

Figure 7. (Color online) Comparison of the experimental voltage-discharge curve at cycle 1000 with the model prediction using parameter values calculated from the power law fits to model parameters fit to voltage-discharge curves for cycles 50 and 100*n* for $n = 1,...,5$. Each red dot is a data point, the blue line is the model prediction, and the 95% predictive intervals were computed based on the parametric uncertainties quantified by pdfs of the model parameters. Similar quality fits and prediction intervals occurred for the other cycles.

good agreement with the experimental data at cycle 1000 (see Fig. 7), indicating that the model was able to predict capacity fade.

Conclusions

The effective solid-phase diffusion coefficients and electrochemical reaction rate constants in positive and negative electrodes and the effective electrolyte diffusion coefficient were estimated and tracked as a function of cycle #. The mathematical analysis indicated that (i) nearly all of the variation in voltage-discharge curves could be explained by changes in only the two model parameters associated with transport and electrochemical kinetics in the negative electrode (Fig. 3b), and (ii) the monotonic reduction in the estimated effective solid-phase diffusion coefficient in the negative electrode due to capacity fade was due to actual changes in the model parameter rather than uncertainties in the parameter estimation resulting from limited parameter identifiability and limited data (Fig. 4). After characterizing uncertainties in the parameters (Table III), the effects of the parameter uncertainties on the voltage-discharge curve were quantified (Fig. 6). Small prediction intervals, as well as comparisons of model predictions with experimental data (Figs. 5–7), provided confidence in the ability of the model to predict capacity fade. Tracking cycle-dependent variations in the effective values for transport and electrochemical kinetics is valid only for a particular protocol of galvanostatic charge and discharge, and is not appropriate for use in the design of lithium-ion batteries with reduced capacity fade.

The proposed approach is appropriate for estimating the lifetime of a lithium-ion battery from past measured voltage-discharge curves. This study considers a battery operating for a consistent set of conditions; it would be useful to assess whether the approach is useful for time-varying discharge conditions (within an allowable window of operations). The proposed approach is computationally efficient enough that it could be integrated into an inexpensive microprocessor for estimating the remaining battery lifetime, based on minimum requirements on the voltage-discharge curve for the battery to be useful in its application. The proposed approach can also provide guidance as to which battery components are likely the primary causes for capacity fade for a battery operating within a specified window of operating conditions. For example, in this study the voltage-discharge curves were sensitive to the negative-electrode parameters which suggested that the capacity fade mechanisms in the negative electrode have a more pronounced effect on the voltage-discharge curves. A designer working to improve the battery designed for this operating condition would focus on modification of the negative-electrode parameters (e.g., geometries, porosity) to reduce the capacity fade.

Acknowledgments

The authors are thankful for the partial financial support of this work by the National Science Foundation under contract numbers CBET-0828002, CBET-0828123, and CBET-1008692, the International Center for Advanced Renewable Energy and Sustainability at Washington University in St. Louis (ICARES), and the U.S. government.

List of Symbols

a_i	specific surface area of electrode i ($i = p, n$), m^2/m^3
$brugg_i$	Bruggman coefficient of region i ($i = p, s, n$)
c	electrolyte concentration, mol/m^3
c_0	initial electrolyte concentration, mol/m^3
$c_{s,i}$	concentration of lithium ions in the intercalation particle of electrode i ($i = p, n$), mol/m^3
$c_{s,i,0}$	initial concentration of lithium ions in the intercalation particle of electrode i ($i = p, n$), mol/m^3
$c_{s,max,I}$	maximum concentration of lithium ions in the intercalation particle of electrode i ($i = p, n$), mol/m^3
D_i	electrolyte diffusion coefficient, m^2/s
$D_{s,i}$	lithium ion diffusion coefficient in the intercalation particle of electrode i ($i = p, n$), m^2/s
F	Faraday's constant, C/mol
I	applied current density, A/cm^2
i_1	solid-phase current density, A/m^2
i_2	solution-phase current density, A/m^2
$i_{0,s}$	exchange current density for the solvent reduction reaction, A/m^2
j_s	solvent reduction current density, mol/m^2s
j_i	wall flux of Li^+ on the intercalation particle of electrode i ($i = n, p$), mol/m^2s
k_i	intercalation/deintercalation reaction rate constant of electrode i ($i = p, n$), $mol/(mol/m^3)$[1,5]
l_i	thickness of region i ($i = p, s, n$), m
M_s	molecular weight of the solvent reaction product, g/mol
n	negative electrode
N	cycle number (dimensionless)
p	positive electrode
r	radial coordinate, m
R	universal gas constant, J/(mol·K)
R_{film}	Initial SEI layer resistance at the negative electrode, $\Omega \cdot m^2$
R_i	radius of the intercalation particle of electrode i ($i = p, n$), m
s	Separator
t_+	Li^+ transference number in the electrolyte
T	absolute temperature, K
U_i	open-circuit potential of electrode i ($i = p, n$), V
U_s	standard potential of the solvent reduction reaction, V
X	spatial coordinate, m
x_{i0}	initial state of charge at the electrode
δ	thickness of the solvent reduction product film, m
δ_0	initial thickness of the solvent reduction product film, m
ε_i	porosity of region i ($i = p, s, n$)
$\varepsilon_{f,i}$	volume fraction of fillers of electrode i ($i = p, n$)
η_i	overpotential driving a reaction, V
η_s	overpotential driving the side reaction, V
κ	ionic conductivity of the electrolyte, S/m
$\kappa_{eff,i}$	effective ionic conductivity of the electrolyte in region i ($i = p, s, n$), S/m
Φ_1	solid-phase potential, V
Φ_2	electrolyte-phase potential, V
ρ_s	density of the solvent reduction product film, g/m^3
σ_i	electronic conductivity of the solid phase of electrode i ($i = p, n$), S/m
$\sigma_{eff,i}$	effective electronic conductivity of the solid phase of electrode i ($i = p, n$), S/m
θ_i	dimensionless concentration of lithium ions in the intercalation particle of electrode i ($\theta_i = c_{s,i}/c_{s,max,i}$)

References

1. G. G. Botte, V. R. Subramanian, and R. E. White, *Electrochim. Acta*, **45**, 2595 (2000).
2. T. F. Fuller, M. Doyle, and J. Newman, *J. Electrochem. Soc.*, **141**, 982 (1994).
3. V. R. Subramanian, V. Boovaragavan, and V. D. Diwakar, Electrochem. Solid-State Lett., **10**, A255 (2007).
4. V. R. Subramanian, V. Boovaragavan, V. Ramadesigan, and M. Arabandi, J. Electrochem. Soc., **156**, A260 (2009).
5. Q. Zhang and R. E. White, *J. Power Sources*, **179**, 793 (2008).

6. M. Doyle, T. F. Fuller, and J. Newman, *J. Electrochem. Soc.*, **140**, 1526 (1993).
7. P. Arora, R. E. White, and M. Doyle, *J. Electrochem. Soc.*, **145**, 3647 (1998).
8. P. Ramadass, B. Haran, P. M. Gomadam, R. White, and B. N. Popov, *J. Electrochem. Soc.*, **151**, A196 (2004).
9. M. Safari, M. Morcrette, A. Teyssot, and C. Delacourt, *J. Electrochem. Soc.*, **157**, A892 (2010).
10. M. Safari, M. Morcrette, A. Teyssot, and C. Delacourt, *J. Electrochem. Soc.*, **157**, A713 (2010).
11. T. Yoshida, M. Takahashi, S. Morikawa, C. Ihara, H. Katsukawa, T. Shiratsuchi, and J. Yamaki, *J. Electrochem. Soc.*, **153**, A576 (2006).
12. V. Ramadesigan, V. Boovaragavan, J. C. Pirkle, and V. R. Subramanian, *J. Electrochem. Soc.*, **157**, A854 (2010).
13. J. van Brakel and P. M. Heertjes, *Int. J. Heat Mass Transfer*, **17**, 1093 (1974).
14. A. Bjorck, *Numerical Methods for Least Squares Problems*, SIAM, Philadelphia (1996).
15. R. Gunawan, M. Y. L. Jung, E. G. Seebauer, and R. D. Braatz, *AIChE J.*, **49**, 2114 (2003).
16. J. V. Beck and K. J. Arnold, *Parameter Estimation in Engineering and Science*, John Wiley & Sons, New York (1977).
17. M. W. Hermanto, N. C. Kee, R. B. H. Tan, M. S. Chiu, and R. D. Braatz, *AIChE J.*, **54**, 3248 (2008).
18. L. Tierney, *Ann. Stat.*, **22**, 1701 (1994).
19. R. E. Caflisch, *Acta Numerica*, **7**, 1 (1998).
20. Z. K. Nagy and R. D. Braatz, *J. Process Control*, **17**, 229 (2007).
21. N. Wiener, *Am. J. Math.*, **60**, 897 (1938).
22. D. L. Ma and R. D. Braatz, *IEEE Trans. Control Syst. Technol.*, **9**, 766 (2001).
23. D. L. Ma, S. H. Chung, and R. D. Braatz, *AIChE J.*, **45**, 1469 (1999).
24. Z. K. Nagy and R. D. Braatz, *J. Process Control*, **14**, 411 (2004).
25. B. J. Debusschere, H. N. Najm, A. Matta, O. M. Knio, R. G. Ghanem, and O. P. Le Maitre, *Phys. Fluids*, **15**, 2238 (2003).
26. http://www.quallion.com, last accessed January 25, 2011.
27. V. R. Subramanian, V. Boovaragavan, V. Ramadesigan, K. Chen, and R. D. Braatz, in *Design for Energy and the Environment: Proceedings of the Seventh International Conference on the Foundations of Computer-Aided Process Design*, M. M. El-Halwagi and A. A. Linninger, Editors, p. 987, CRC, Boca Raton (2009).
28. A. Coniglio, A. Fierro, H. J. Herrmann, M. Nicodemi, and Ebooks Corporation., Unifying Concepts in Granular Media and Glasses: From the Statistical Mechanics of Granular Media to the Theory of Jamming, Elsevier, Burlington (2004).